VEGETATION DETECTION IN MULTISPECTRAL REMOTE SENSING IMAGES: PROTECTIVE ROLE-ANALYSIS OF VEGETATION IN 2004 INDIAN OCEAN TSUNAMI

Rajlaxmi Chouhan [a, *], Neeraj Rao [b]

[a, b] PDPM Indian Institute of Information Technology, Design & Manufacturing Jabalpur, (India)
[a] rajlaxmi1020203@iiitdmj.ac.in, [b] neerajr@iiitdmj.ac.in

KEY WORDS: Vegetation detection, Remote sensing images, NDVI, Protective role of vegetation, Indian Ocean Tsunami

ABSTRACT:

The vegetation response to environment is very sensitive and not only affects the ecological balance and climate but has also been found to be effective barrier against natural disasters. This paper shows how differences between the visible red and near-infrared (NIR) bands of a LANDSAT image can be used to identify areas containing significant vegetation. It uses a LANDSAT Thematic Mapper image covering part of Paris, France, made available courtesy of Space Imaging, LLC. Seven spectral bands are stored in one file in the Erdas LAN format. It also describes how remote sensing techniques and vegetation analysis were used to study the effect of mangroves and other woody coastal vegetation as a protective measure against the 2004 Indian Ocean Tsunami.

1. INTRODUCTION

Remote Sensing is the science and art of acquiring information (spectral, spatial, and temporal) about material objects, area, or phenomenon, without coming into physical contact with the objects, or area, or phenomenon under investigation. Without direct contact, some means of transferring information through space must be utilized. In remote sensing, information transfer is accomplished by use of electromagnetic radiation (EMR). EMR is a form of energy that reveals its presence by the observable effects it produces when it strikes the matter. EMR is considered to span the spectrum of wavelengths from 10-10 mm to cosmic rays up to 1010 mm, the broadcast wavelengths, which extend from 0.30-15 mm [Gonzales 2007].

In respect to Wavelength Regions:
Remote Sensing is classified into three types in respect to the wavelength regions

1. Visible and Reflective Infrared Remote Sensing.
2. Thermal Infrared Remote Sensing.
3. Microwave Remote Sensing.

A significant advance in sensor technology stemmed from subdividing spectral ranges of radiation into bands (intervals of continuous wavelengths), allowing sensors that produce several bands of differing wavelengths to form multispectral images.

Digital image processing of satellite data provides tools for analysing the image through different algorithms and mathematical indices. Based on reflectance characteristics, indices have been devised to highlight features of interest on the image. There are several indices for highlighting vegetation-bearing areas on a remote sensing scene. Normalized Difference Vegetation Index (NDVI) is a common and widely used index. Methods have been developed to detect vegetation from 3-D point clouds [Vandapel, 2004; Macedo, 2000], but there is still significant room for improvement, particularly at longer ranges where the limited viewpoint of onboard sensors, reflection of the laser pulses away from the scanner, laser beam divergence, and partial occlusion by other objects make it difficult to obtain point clouds of sufficient quality and density. Fortunately there are well-established techniques for measuring chlorophyll content using a multi-spectral camera [Clark, 2003; Crippen, 1990; Huete, 1988; Jordan, 1969; Kauth, 1976; Kreigler, 1969; Willstatter, 1913; Richardson, 1977] that have been developed for satellite-based remote sensing. In this paper, an NDVI-based approach has been applied after a pre-processing a multispectral remote sensing image to calculate area under vegetation using a threshold value.

2. FINDING VEGETATION IN A MULTISPECTRAL REMOTE SENSING IMAGE

Variations in the reflectivity of surface materials across different spectral bands provide a fundamental mechanism for understanding features in remotely-sensed multispectral imagery. Chlorophyll is the key factor in reflectivity of vegetation. It absorbs strongly in red, giving rise to our visible observation that healthy vegetation is green. But chlorophyll reflects most strongly in very near-infrared (VNIR) just beyond the visible (Fig. 1) [Bradley, 2007].

NDVI which varies from -1 (blue sky) to 1 (chlorophyll-rich vegetation) can be calculated using (NIR-Red)/(NIR+Red) [Kreigler, 1969].

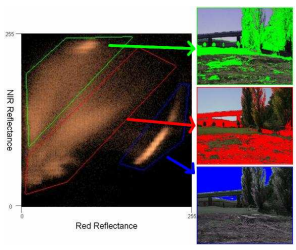

* Corresponding author

Figure 1. Scatter plot of NIR reflectance vs. red reflectance for all pixels in a typical image. Different regions in the scatterplot correspond to different types of materials in the image. Pixels in the green region correspond to vegetation (top image), pixels in the red region are mainly soil and man-made structures (middle image), and pixels in the blue region correspond to sky (bottom image).

2.1 Algorithm for Vegetation Detection

The following algorithm has been followed for detection of vegetation in a multispectral remote sensing image. Results obtained from implementation using MATLAB™ computing tool [MATLAB, 2008] have been shown along with description of every step

Step 1: Import CIR bands from a BIL image file.

The LAN file, paris.lan, contains a 7-band 512-by-512 Landsat image. A 128-byte header is followed by the pixel values, which are band interleaved by line (BIL) in order of increasing band number. They are stored as unsigned 8-bit integers, in little-endian byte order.

Band No.	**Name**	**Wavelength (μm)**	**Characteristics & Uses**
1	Visible blue	0.45-0.52	Maximum water penetration
2	Visible green	0.52-0.60	Good for measuring plant vigour
3	**Visible red**	**0.63-0.69**	**Vegetation discrimination**
4	Near Infrared	0.76-0.90	Biomass and shoreline mapping
5	Middle infrared	1.55-1.75	Moisture content of soil and vegetation
6	Thermal infrared	10.4-12.5	Soil moisture; thermal mapping
7	Middle infrared	2.08-2.35	Mineral mapping

Figure 2. Thematic bands of NASA's LANDSAT satellite

Thematic Mapper 4, 3, and 2 bands cover the near infrared (NIR), the visible red, and the visible green parts of the electromagnetic spectrum [Gonzales, 2007]. When they are mapped to the red, green, and blue planes, respectively, of an RGB image the result is a standard color-infrared (CIR) composite.

Step 2: Enhance the CIR composite with a decorrelation stretch.

It's helpful, before analyzing the CIR composite, to enhance it for more effective visual display. Because of the subtle color differences in the original composite, a decorrelation stretch is suitable. By analyzing differences between the NIR and red bands, we can quantify this contrast in spectral content between vegetated areas and other surfaces such as pavement, bare soil, buildings, or water.

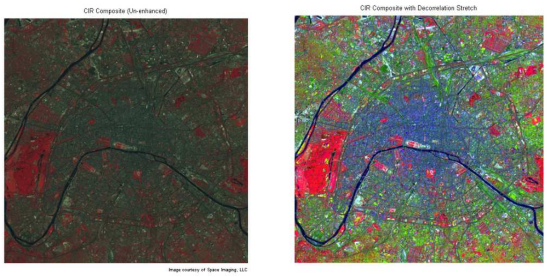

(a) (b)

Figure 3 (a) CIR Composite (Un-enhanced) (b) CIR Composite with decorrelation Stretch. Much of the image appearance is due to the fact that healthy, chlorophyll-rich vegetation has a high reflectance in the near infrared. Because the NIR band is mapped to the red channel in our composite, any area with a high vegetation density appears red in the display. A noticeable example is the area of bright red on the left edge, a large park (the Bois de Boulogne) located west of central Paris within a bend of the Seine River (Fig 3 (a)-(c)).

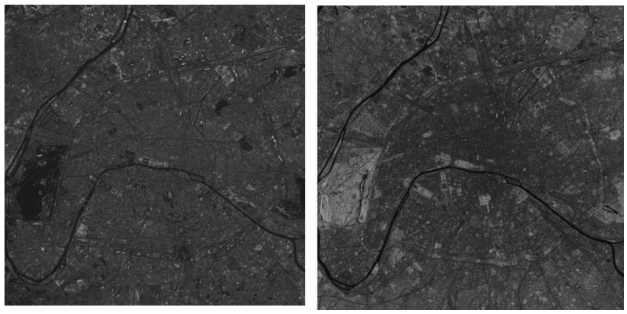

Figure3(c) Visible red band Figure 3(d) Near IR band

Step 3: Construct an NIR-red spectral scatter plot

A scatter plot is a natural place to start when comparing the NIR band (displayed as red) with the visible red band (displayed as green). It's convenient to extract these bands from the original CIR composite into individual variables (Fig. 4).

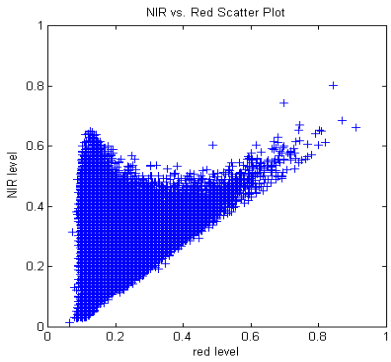

Figure 4. The appearance of the scatter plot of the Paris scene is characteristic of a temperate urban area with trees in summer foliage. There's a set of pixels near the diagonal for which the NIR and red values are nearly equal. This "gray edge" includes features such as road surfaces and many rooftops. Above and to the left is another set of pixels for which the NIR value is often well above the red value. This zone encompasses essentially all of the green vegetation.

Step 4: Compute vegetation index via MATLAB array arithmetic.

The Normalized Difference Vegetation Index (NDVI) is motivated by the observation that the difference between the NIR and red should be larger for greater chlorophyll density. It takes the (NIR - red) difference and normalizes it to help balance out the effects of uneven illumination such as the shadows of clouds or hills. In other words, on a pixel-by-pixel basis subtract the value of the red band from the value of the NIR band and divide by their sum. Very low values of NDVI (0.1 and below) correspond to barren areas of rock, sand, or snow. Moderate values represent Shrub and grassland (0.2 to 0.3), while high values indicate temperate and tropical rainforests (0.6 to 0.8).

Step 5: Locate vegetation -- threshold the NDVI image

In order to identify pixels most likely to contain significant vegetation, a simple threshold to the NDVI image is applied (Fig. 3(e)-(f)).

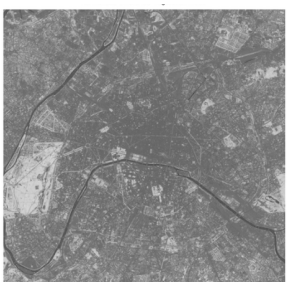

Figure 3(e)

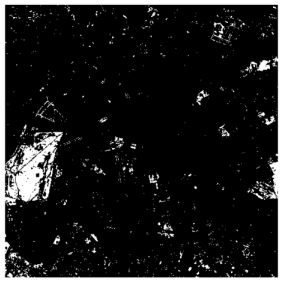

Figure 3(f)

Fig 3(e) Normalized Difference Vegetation Index (f) NDVI with Threshold Applied. The Seine River appears very dark in the NDVI image. The large light area near the left edge of the image is the park (Bois de Boulogne) noted earlier. The park and other smaller areas of vegetation appear white by default when displaying the logical (binary) image.

Step 6: Link spectral and spatial content

To link the spectral and spatial content, you can locate above-threshold pixels on the NIR-red scatter plot (Fig. 3(g)), re-drawing the scatter plot with the above-threshold pixels in a contrasting color (green) and then re-displaying the threshold NDVI image using the same blue-green color scheme as in Figure 3(f). As expected, the pixels having an NDVI value above the threshold appear to the upper left of the rest and correspond to the redder pixels in the CIR composite displays.

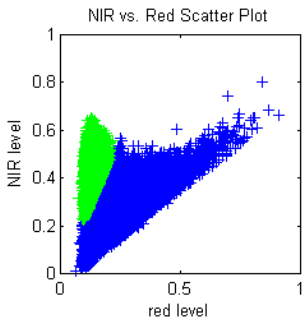

Figure 3(g)

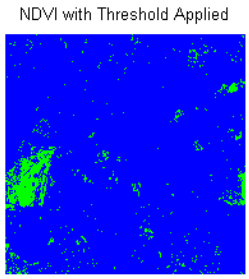

Figure 3(h)

Percentage of Vegetation is calculated by ratio of number of while pixels in binary image to total number of pixels in NIR image. It was found to be **5.2204%.**

3. APPLICATION OF VEGETATION ANALYSIS FROM REMOTE SENSING IMAGES

3.1 Protective Role Of Mangrove Forests in 2004 Indian Ocean Tsunami

This section describes how remote sensing techniques were used to study the effect of mangroves and other woody coastal vegetation as a protective measure against the 2004 Indian Ocean Tsunami. Remote sensing made it possible to compare pre- and post-Tsunami images of large areas [Olwig, 2007] . A study site was selected based on medium resolution Landsat imagery and existing topographic maps. Selection criteria included substantial damages reported, presence of woody vegetated and non-vegetated shorelines, homogeneous bathymetry and good coverage of pre and post-Tsunami satellite imagery. The Pichawaram mangrove, Tamil Nadu, India, matched these criteria. Pre- and post-Tsunami Ikonos and QuickBird images were compared through the visual interpretation and multispectral analysis of pre-Tsunami coastal vegetation and post-Tsunami damage. The results were validated in the field.

As an aid to humanitarian and noncommercial efforts to reduce Tsunami vulnerability, the UN initiative UNOSAT made available several satellite images from the areas affected by the Tsunami including the area around Pichawaram. These data consisted of the blue, green and NIR 4m bands from an Ikonos satellite image of 29 December 2004, only a few days after the Tsunami. The blue, green, red, NIR and panchromatic bands from a QuickBird satellite image, covering part of the scene of 31 December 2004, were also available from UNOSAT, A pan-sharpened 0.6m QuickBird satellite image of 4 May 2003, covering the Pichawaram area, was therefore also acquired.

3.1.1 The study site

The study site covers about 20 km of coastline along the eastern coast of Tamil Nadu, India, (11’279” N, 79’489”E to 11’169” N, 79’519” E) (see Figure 1 and 2). The Pichawaram mangrove is situated in the northern part of the study site. The rest of the site is comprised of agriculture and shrimp farms. The mangrove is connected to the Coleroon estuary in the south through a number of backwater canals.

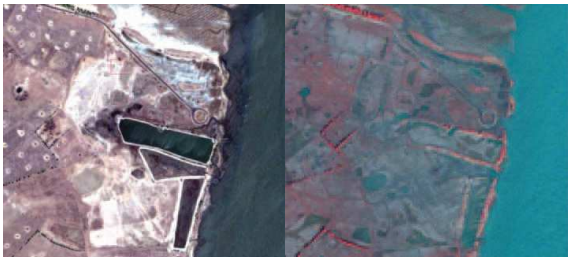

Figure 4. These images show the severely damaged agricultural area southeast of T. S.Pettai. Pre-Tsunami (a) and post-Tsunami (b) images.

3.1.2 Visual interpretation

Figures 4, 5 and 6 provide examples of how the pre- and post-Tsunami images were interpreted. Figure 4 shows the severely damaged agricultural area southeast of T. S. Pettai. The post-Tsunami image (Fig. 4(b)) shows that all features in the

agricultural land have either disappeared or are blurred compared to the pre- Tsunami image (Fig. 4(a)).

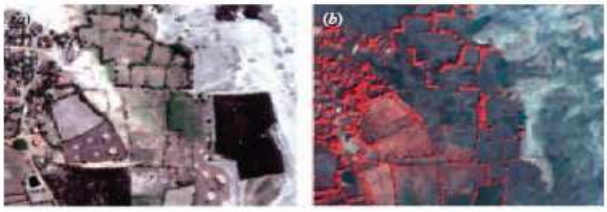

Figure 5. These images show the eastern part of the undamaged hamlet of Kodiyampalayam and the severely damaged agricultural areas southeast of the hamlet; (a) pre-Tsunami, (b) post-Tsunami

3.1.3 Multispectral Interpretation

A map showing the damage and the presence and absence of the woody vegetation is shown in Figure 6. The white-contour indicates the extent of the study area, the dark green refers to dense woody vegetation, the light-green to open woody vegetation, the red to areas severely damaged by the Tsunami, the red-striped to areas only partially damaged and the dotted blue to areas inundated by water, but otherwise undamaged.

The large dark-green area in the northern part of the map is the Pichawaram mangrove. Five hamlets are situated near this mangrove. Two of them, Kannagai Nagar and Pillumedu, are located on the coast whereas three hamlets, T. S. Pettai, Vadakku Pichawaram and Therkku Pichawaram, are behind the mangrove. Ground truth data showed that the two hamlets on the coast were completely destroyed, whereas the three hamlets behind the mangrove suffered no destruction at all. Just north of these hamlets (and west and north-west of Kannagai Nagar), areas at the same distance from the sea, but without protection from woody vegetative, were inundated.

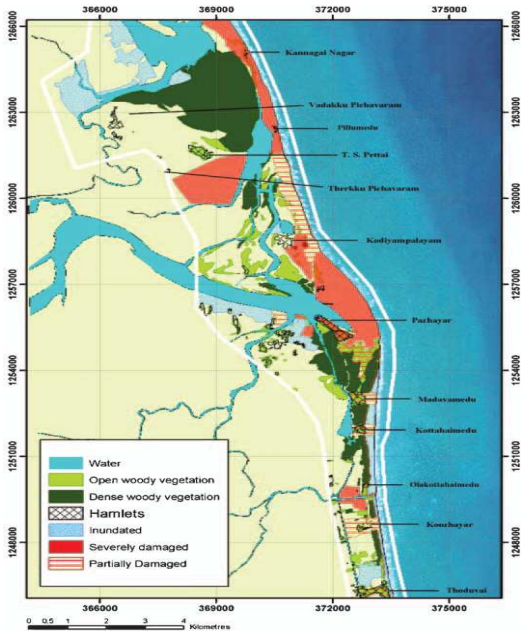

Figure 6. Map depicting the extent of the damage and the areas covered by woody vegetation.

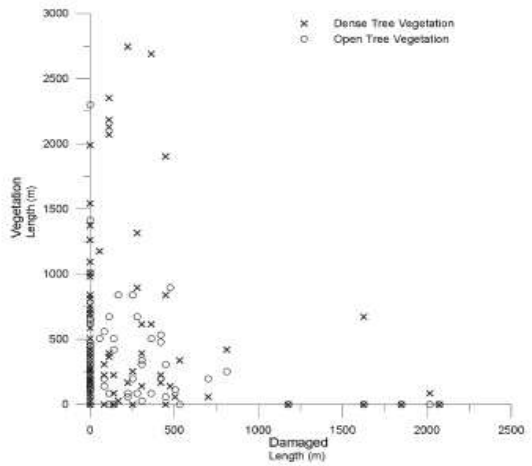

Figure 7. One hundred profiles were established along the coast. These were oriented north-east southwest to match the direction of tsunami wave.

3.1.4 Inferences from case study

The analysis (Fig. 7) showed that mangrove forests and coastal shelterbelts provided protection from the Tsunami. This was concluded from analyzing the spatial distribution of damage relative to woody vegetation along the coast as well as transects detailing the amount of damage behind the coastline and the coastal woody vegetation. In various other cases, like Kosi flood and other natural disasters, remote sensing applications and feature detection greatly contribute to humanitarian aid and disaster management.

4. CONCLUSION

The percentage of vegetation in the given studied landsat image was found to be 5.2204 % at NDVI threshold of 0.4. The algorithm developed gives very good results for vegetation varying in densities and also for scattered vegetation from a multispectral remote sensing image. By varying the value of threshold index varying densities of vegetation coverage can be detected.

Apart from studies of agricultural needs and crop patterns, the vegetation analysis can be used in the events of unfortunate natural disasters to provide humanitarian aid and damage assessment and also to device new protection strategies.

5. FUTURE WORK

With slight modifications in the code for vegetation calculation, like changing the bands used to form composite, other features like water, biomass, shoreline mapping and moisture absorption can also be calculated.

6. REFERENCES

Bradley, D.M., Unnikrishnan, R., and Bagnell, J., 2007. Vegetation Detection for Driving in Complex Environments. In Proc. of IEEE Int. Conf. of Robotics and Automation, pp. 503-508.

Clark, R.N., Swayze, G. A., Livo, K. E., Kokaly, R. F. Sutley, S. J., Dalton, J. B., McDougal, R. R., and Gent, C., 2003. Imaging spectroscopy: Earth and planetary remote sensing with

the usgs tetracorder and expert systems, J. Geophys. Res. December 2003.

Crippen, R. E., 1990. Calculating the vegetation index faster," Remote Sensing of Environment, 34, pp. 71–73.

F. J. Kreigler, W. A. Malila, R. Nalepka, and W. Richardson, 1969. Preprocessing transformations and their effects on multispectral recognition. In Proc. of the Sixth International Symposium on Remote Sensing of Environment, Ann Arbor, MI, pp. 97–131.

Gonzalez, R.C., Woods, R.E., 2000. *Digital Image Processing*. Upper Saddle River, Prentice Hall, Inc., New Jersey.

Huete, A. R., 1988. A soil adjusted vegetation index (savi). Remote Sensing of Environment, 25, pp. 295–309.

Jordan, C. F., 1969. Derivation of leaf area index from quality measurements of light on the forest floor. Ecology, 50, pp. 663–666.

Kauth, R. J., and Thomas, G. S., 1976. The tasseled cap - a graphic description of the spectral-temporal development of agricultural crops as seen by landsat. In LARS: Proceedings of the Symposium on Machine Processing of Remotely Sensed Data, West Lafayette, IN, pp. 4B–14–4B–51.

Kroeger, G.C., 1995. Geologic Remote Sensing and Multispectral Image Processing. Report, Keck Geology Symposium, 8th Keck Symposium Volume, pp. 125-130.

Macedo, J., Manduchi, R., and Matthies, L., 2000. Ladar-based discrimination of grass from obstacles for autonomous navigation. In Proc. of the International Symposium on Experimental Robotics, Honolulu, HA.

MATLAB Image Processing Toolbox User Manual, 2008, MathWorks, Inc., MA.

Olwig, M. F., Sørensen, M. K., Rasmussen, M. S., Danielsen, F., Selvam, V., Hansen, L. B., Nyborg, L., Vestergaard, K. B., Parish, F., and Karunagaran, V. M., 2007. Using remote sensing to assess the protective role of coastal woody vegetation against tsunami waves. *International Journal of Remote Sensing*, 28(13), pp. 3153 – 3169.

Richardson, A. J., and Wiegand, C. L., 1977. Distinguishing vegetation from soil background information. Photogrammetric Engineering and Remote Sensing, 43, pp. 1541–1552.

Vandapel, V., and Hebert, M., 2004. Natural terrain classification using 3-d ladar data," in IEEE Intl. Conf. on Robotics and Automation (ICRA).

Willstatter, R., and Stoll, A., 1913. Utersuchungenuber Chlorophyll. Springer, Berlin.